

# Duration of Individual Relativistic Electron Microbursts: A Probe Into Their Scattering Mechanism

M. Shumko<sup>1,2</sup>, L.W. Blum<sup>3</sup>, and A.B. Crew<sup>4</sup>

<sup>1</sup>NASA's Goddard Space Flight Center, Greenbelt, Maryland, USA

<sup>3</sup>Universities Space Research Association, Columbia, Maryland, USA

<sup>3</sup>University of Colorado Boulder, Boulder, Colorado, USA

<sup>2</sup>Johns Hopkins University Applied Physics Laboratory, Laurel, Maryland, USA

## Key Points:

- We identified relativistic microbursts observed by the SAMPEX satellite and quantified their duration
- The microburst duration interquartile range is 70-140 ms and shows trends in AE, L-shell, and MLT
- [Which one do you like more. This version?](#) In MLT, microburst durations are shortest at midnight and longest at noon—a similar trend to chorus element durations.
- [Or this version?](#) In MLT, microburst duration doubles between midnight and noon—a trend similar to chorus element durations.

## Abstract

We used the Solar Anomalous and Magnetospheric Particle Explorer (SAMPEX) to identify and quantify the duration of  $> 1$  MeV electron microbursts. We investigated trends in the microburst duration as a function of geomagnetic activity, L-shell, and magnetic local time (MLT)—with the clearest trend in MLT. The median microburst duration doubles from 80 milliseconds at midnight to 160 milliseconds noon MLT. This trend is similar to the whistler mode chorus rising tone element duration trend, but theory does not conclusively predict what chorus wave properties control microburst duration.

## Plain Language Summary

*Does this summary read well now?*

Energetic electron microbursts are an intense form of naturally occurring particle precipitation from the outer Van Allen Radiation Belt into Earth’s atmosphere. Microbursts are observed in, or just above, Earth’s atmosphere, and are characterized by their short duration in time series data, often defined to be less than a second. The impact of microburst precipitation on Earth’s atmosphere is uncertain, but has been predicted to substantially degrade Mesospheric Ozone through the production of Odd Nitrogen and Odd Hydrogen molecules. Besides their environmental impact, we don’t comprehensively understand how plasma waves, such as whistler mode chorus waves, scatter microbursts into our atmosphere. Therefore, in this study we quantified the duration of microbursts and used it as a proxy to understand how microbursts are scattered by these waves. We found that the microburst and chorus wave durations are correlated: their duration roughly doubles between the anti-sunward and sunward regions of the outer radiation belt.

## 1 Introduction

Earth’s outer Van Allen radiation belt electron population is in constant flux, controlled by processes such as, radial transport, injections from the magnetotail, magnetopause shadowing, and local heating and loss into Earth’s atmosphere due to wave-particle interactions (e.g. Ripoll et al., 2020, and references within). Whistler mode chorus (WMC) is one type of plasma wave, characterized by short,  $\approx 100$  millisecond (ms) rising tone elements, that plays a dual role in electron dynamics: accelerate electrons from 10s of keV to MeV energies, and pitch angle scatter electrons into the atmosphere (e.g. Li, Thorne, Angelopoulos, Bonnell, et al., 2009; Thorne, 2010; Horne & Thorne, 2003; Summers, 2005). One form of electron precipitation believed to be generated by WMC are microbursts: a subsecond intense increase of electrons. Microbursts were first observed by balloons in Earth’s upper atmosphere, and later by satellites in low Earth orbit (LEO), and recently at high altitude near the magnetic equator (e.g. Winckler et al., 1962; Anderson & Milton, 1964; Blake et al., 1996; Lorentzen et al., 2001; O’Brien et al., 2003; Douma et al., 2017; Kurita et al., 2016; Shumko et al., 2018).

Microburst electron energies span multiple orders of magnitude from tens of keV observed by, for example, Datta et al. (1997); to  $> 1$  MeV observed by the Solar Anomalous Magnetospheric Particle Explorer (SAMPEX) by Blum et al. (2015). Microbursts are predominately observed outside the plasmapause on the radiation belt footprints,  $L \approx 4 - 8$ , and in the midnight to morning Magnetic Local Times (MLT) ( $\approx 0 - 12$  hours MLT) (Lorentzen et al., 2001; Blum et al., 2015; O’Brien et al., 2003; Douma et al., 2017). While microbursts are observed under all geomagnetic conditions, Douma et al. (2017) showed that microburst occurrence frequency dramatically increases with the Auroral Electrojet (AE) index, and O’Brien et al. (2003) showed a similar trend with the microburst frequency with the Disturbance storm time index phase.

The relative impact of energetic electron precipitation on the ionization of Earth's atmosphere and the depletion of radiation belt electrons is uncertain, but is estimated to be substantial. Duderstadt et al. (2021) showed observations that suggest that electron precipitation can significantly impact atmospheric composition. The authors estimated a 20-30% increase in atmospheric Odd Nitrogen ( $\text{NO}_x$ ), leading to a 1% decrease in Ozone ( $\text{O}_3$ )—substantial enough to affect the radiative balance in the upper atmosphere. More specifically, the impact of microbursts alone is estimated to be substantial. Microbursts can deplete the outer radiation belt electrons in as little as a few hours, and models predict depletions of up to 20% of upper mesospheric  $\text{O}_3$  (O'Brien et al., 2004; Thorne et al., 2005; Douma et al., 2019; Breneman et al., 2017; Seppälä et al., 2018).

Electron microbursts are widely believed to be scattered by chorus waves. They were associated early on, due to the similar duration of microbursts and chorus rising tone elements, and a similar occurrence distributions in MLT (e.g. Lorentzen et al., 2001). Furthermore, Breneman et al. (2017) directly linked a chorus rising tone element to a microburst observed by the Focused Investigation of Relativistic Electron Bursts: Intensity, Range, and Dynamics CubeSats (FIREBIRD-II; Crew et al. (2016); Johnson et al. (2020)) during a close magnetic conjunction.

A natural follow-on question is how are microbursts scattered. For example, it is still unclear if relativistic ( $> 1$  MeV) microbursts are scattered via cyclotron resonance at high magnetic latitudes, or a higher resonance harmonic near the magnetic equator (Lorentzen et al., 2001). One way to address this question is to study for how long microburst electrons are in resonance with a chorus wave. The resulting microburst duration, i.e. the microburst width in the time series data, is a probe into the conditions necessary to scatter microburst electrons. Therefore, we used microbursts observed by the SAMPEX satellite to quantify the distribution of relativistic microburst duration. In this letter, we quantify the duration distribution of microbursts as a function of L-shell, MLT, and the Auroral Electrojet. We then compare these results to prior chorus rising tone element studies, and a chorus-electron test particle model.

## 2 Instrumentation

We use the  $> 1$  MeV electron count data, taken by the Heavy Ion Large Telescope (HILT) instrument (Klecker et al., 1993), onboard the SAMPEX satellite (Baker et al., 1993).

SAMPEX was launched in July 1992 and reentered Earth's atmosphere in November 2012. It was in a 520x670 km,  $82^\circ$  inclination low Earth orbit. In general, SAMPEX had two pointing modes: spin and orbit rate rotation (zenith pointing) modes. To avoid the compounding effects due to the variable pitch angles sampled in the spin mode, we only used the zenith pointing mode data. The International Geomagnetic Reference Field (Thébault et al., 2015, IGRF) magnetic field model was used to derive the geomagnetic coordinates.

The HILT instrument consisted of a large rectangular chamber with the aperture on one end, and 16 solid state detectors on the other. We used the HILT electron data taken between 1997 and 2012 (state4 in the data archive). The electron counts were accumulated from all of the solid state detectors at a 20 ms cadence.

## 3 Methodology

We first identified microbursts. We then fit every microburst's time series to a model, consisting of a Gaussian superposed with a straight line, to quantify the duration for each microburst.



**Figure 1.** Examples of relativistic microbursts are shown by the black lines, and the fits are shown by the dashed red lines. The fit’s full width at half maximum (FWHM) and the  $\bar{R}^2$  goodness of fit metric is annotated in each panel. Microbursts with  $\bar{R}^2 > 0.9$  were used for this study. The major time ticks are at every second, while the minor ticks are at every 100 milliseconds.

### 3.1 Microburst Identification

We identified microbursts using the burst parameter defined by O’Brien et al. (2003) and used in numerous other microburst studies with SAMPEX (e.g. Douma et al., 2017). Assuming Poisson probability for the observed electron counts, the burst parameter is the number of standard deviations of a foreground signal above the background, expressed as

$$n_{\sigma} = \frac{N - A}{\sqrt{A + 1}} \quad (1)$$

where  $N$  is the number of foreground electron counts, and  $A$  is the centered running average background counts. The 1 in the denominator prevents a division by 0 error. In O’Brien et al. (2003), and in the results in this study,  $N$  was summed over 100 ms and is called  $N_{100}$ , while  $A$  was summed over 500 ms and is likewise called  $A_{500}$ . Henceforth, we specify the time windows with subscripts for  $N$  and  $A$ . Times when  $n_{\sigma} > 10$  are classified as burst times, and the peak time in each continuous burst time interval is saved to the microburst data set. With  $A_{500}$  and  $N_{100}$ , we detected a total of 256,764 microbursts over the 15 year period from 1997 to 2012. Four examples of microbursts are shown in Fig. 1 by the solid black curves.

### 3.2 Quantify Microburst Duration by Fitting

We estimated the microburst duration using two methods that yielded similar results: the duration at half of the microburst’s topographic prominence and the full width at half maximum (FWHM) from a fit.

The topographic prominence is a simple and robust method to estimate the microburst duration used to identify curtains, a similar-looking type of precipitation (Shumko et al., 2020). It is defined as the duration at half of the microburst’s topographic prominence: the height of the microburst relative to the maximum of the two minima on either side of the microburst peak. On each side of the microburst peak, the minima are searched for between the microburst and a higher peak on that side. While the topographic prominence method of estimating microburst durations is simple and robust, one of its downsides is its inability to automatically verify that the duration is representative of a single microburst. Therefore, we also fit microbursts with a Gaussian, and used the  $R^2$  goodness of fit metric to filter out bad duration estimates. Thus, we exclude events that are a superposition of multiple microbursts—a source of bias.

We assumed a fit model consisting of a Gaussian superposed with a straight line. The Gaussian models the shape of the microburst; the linear trend models the background electrons that are either trapped or quasi-trapped in the drift loss cone. This model is defined as:

$$c(t|A, t_0, \sigma, c_0, c_1) = Ae^{-\frac{(t-t_0)^2}{2\sigma^2}} + c_0 + c_1t \quad (2)$$

where  $A$ ,  $t_0$ , and  $\sigma$  are the Gaussian amplitude, center time, and standard deviation;  $c_0$  and  $c_1$  are the linear background count intercept and slope. The fit was over an interval of HILT data, the maximum of: 4x topographic prominence width or 500 ms. A challenge to any robust and automated nonlinear regression algorithm is guessing the initial parameters. The initial parameter guesses for the Gaussian are provided by the topographic prominence and topographic duration estimates. The two linear trend initial parameters were:  $c_0 = \text{median}(\text{counts})$  and  $c_1 = 0$ . The optimal fit parameters were found using scipy's `curve_fit()` function in Python. We defined the microburst duration as the FWHM of the microburst peak, defined by

$$\text{FWHM} = 2\sqrt{2\ln 2}\sigma. \quad (3)$$

To evaluate the fit, we used the  $R^2$  goodness of fit metric.  $R^2$  is defined as

$$R^2 = 1 - \frac{SS_{res}}{SS_{mean}} = 1 - \frac{\sum (c_i - f_i)^2}{\sum (c_i - \bar{c})^2} \quad (4)$$

where  $SS_{res}$  is the sum of the squared residuals between the observed counts  $c_i$  and the fit counts  $f_i$  for each time step, and likewise  $SS_{mean}$  is the sum of the squared residuals between  $c_i$  and the mean of the counts,  $\bar{c}$ .

One interpretation of  $R^2$ : fractionally how much better the variance in the data is explained by the model fit, compared to the null hypothesis horizontal line at  $\bar{c}$ .  $R^2$  varies from 1 for a perfect fit, to  $-\infty$  for poor fits (a fit can be much worse than the mean null hypothesis).

To account for overfitting, we used the adjusted  $R^2$ ,  $\bar{R}^2$ , defined as

$$\bar{R}^2 = 1 - (1 - R^2) \frac{n - 1}{n - p - 1} \quad (5)$$

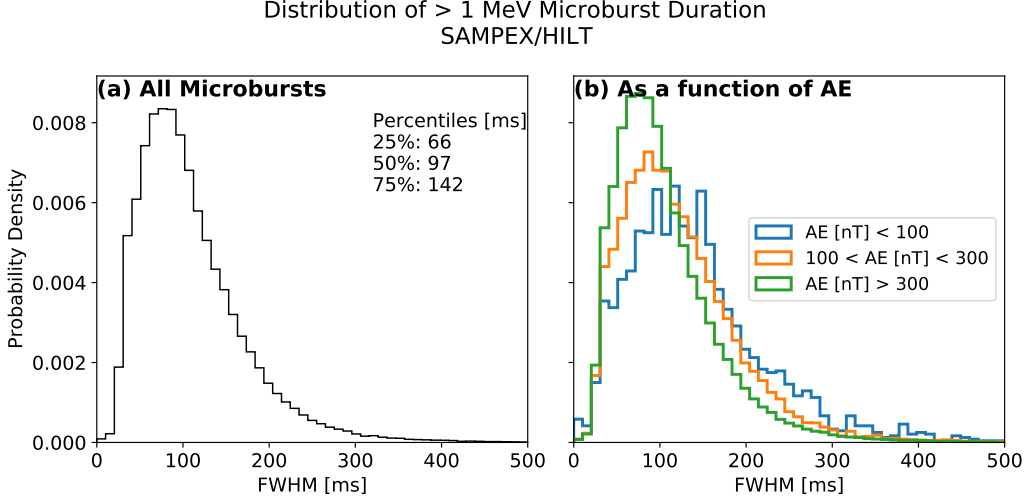
where  $n$  is the number of data points fit, and  $p$  is the number of parameters. Intuitively,  $n - 1$  is the number of degrees of freedom for the null hypothesis, and  $n - p - 1$  is the degrees of freedom for the fit model. Fits with  $\bar{R}^2 > 0.9$  are considered good and are analyzed. As a check, we compared the microburst duration estimated with the prominence and fit methods. [Does the following sentence make more sense now?](#) We first chose an agreement criterion between the two methods as a duration within 25%; together with the  $\bar{R}^2 > 0.9$  constraint, 85% of microbursts satisfied this criterion.

Figure 1a shows an example of two superposed microbursts that had a fit  $\bar{R}^2 = 0.83$  that were excluded from this study. On other hand, microbursts in Fig. 1b-d had  $\bar{R}^2 > 0.9$  and were included in the following analysis.

Lastly, Fig. 1c,d demonstrate the necessity of the linear fit to account for the changing background. The linear fit accounts for the non-zero mean background counts and the uneven amplitudes at the edges of the Gaussian. Of the 256,764 detected microbursts, 109,231 have  $\bar{R}^2 > 0.9$  and are used for the remainder of this study.

## 4 Results

We used the well-fit microbursts to quantify the distribution of microburst duration (FWHM) as a function of the Auroral Electrojet index, L-shell and MLT. We begin with the overall microburst distribution.



**Figure 2.** Panel a shows the distribution of all microburst full width at full maximum (FWHM). Panel b shows the distribution of all microbursts, categorized by the Auroral Electrojet (AE) index into three bins:  $AE < 100$ ,  $100 < AE < 300$ , and  $AE > 300$ , in units of nanotesla. The median microburst duration is 130 ms for the  $AE < 100$  ( $2.4 \times 10^3$  microbursts), 111 ms for the  $100 < AE < 300$  ( $1.8 \times 10^4$  microbursts), and 95 ms for the  $AE > 300$  ( $9.3 \times 10^4$  microbursts) bins.

Figure 2a shows the distribution of all well-fit microbursts. This distribution is strongly peaked with 97 ms median duration. The interquartile range spans about a factor of two in microburst duration, from 66 to 142 ms.

We then investigated the dependence of microburst duration as a function of geomagnetic activity. To be consistent with many prior wave and microburst studies, we use the AE index to quantify the level of geomagnetic disturbance. We adopt the same three AE intensity levels used in prior studies, such as Li, Thorne, Angelopoulos, Bortnik, et al. (2009), Douma et al. (2017), and Meredith et al. (2020):  $AE < 100$ ,  $100 < AE < 300$ , and  $AE > 300$ , in units of nanotesla (nT). Figure 2b shows the distribution of microburst duration for the three AE categories. The distributions are qualitatively similar, gradually narrowing and shifting to shorter durations with increasing AE. The median microburst duration decreases from 130 ms for  $AE < 100$  to 95 ms for  $AE > 300$ .

Lastly, Figs. 3 and 4 show the microburst duration as a function of L and MLT. Figure 3a-c shows the joint distributions, split up into the 25th, 50th, and 75th percentiles; Figure 4 shows the marginalized distributions as a function of L or MLT.

Figure 3 shows that the microburst duration trend is nearly identical for the different percentiles, and thus for simplicity we focus on the median distribution in Fig. 3b. In MLT, the median microburst duration increases by roughly a factor of two: from 80 ms at midnight to 160 ms at noon. In L-shell, the median microburst duration slightly increases with L-shell, and is most apparent near midnight MLT.

To disentangle the L and MLT distributions, Fig. 4 shows the marginalized distributions; MLT was marginalized out in Fig. 4a and L-shell was marginalized out in Fig. 4b. Figure 4a shows a slight broadening of the microburst duration at higher L-shells—

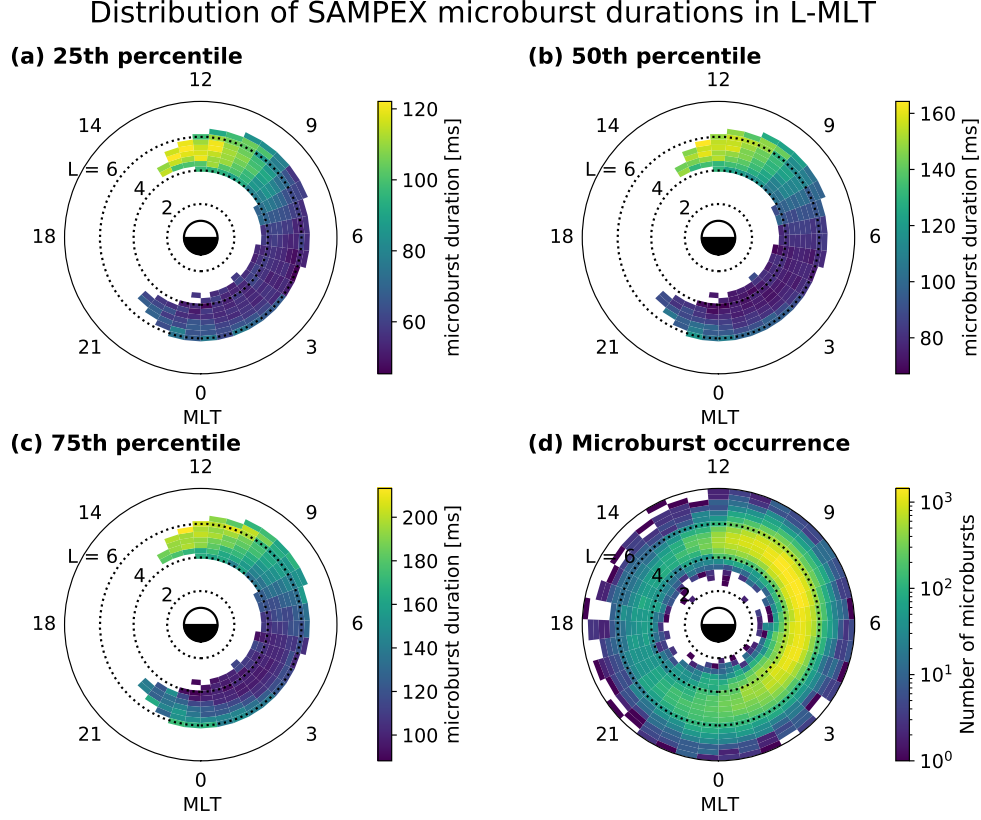


**Figure 3.** The joint distributions of microburst duration (FWHM) as a function of L-Shell and MLT. Panels a-c show the 25th, 50th, and 75th duration percentiles in each L-MLT bin. The white bins in panels a-c have less than 100 microbursts and are statistically insufficient. Lastly, panel d shows the distribution of the number of microbursts, with the white bins containing 0 microbursts.

in contrast to Fig. 4b, that clearly shows the microburst duration increase from midnight to noon MLT.

## 5 Discussion and Conclusions

We first discuss a possibility that the burst parameter is less sensitive to microbursts with longer durations and is therefore not detecting them. Recall from Section 3.1 that  $A$  is the running average counts, centered on the foreground counts  $N$ , and the burst parameter,  $n_\sigma \sim N - A$ . Now consider the following hypothesized scenario. Given a microburst with a 500 ms duration and the burst parameter centered on the peak,  $A_{500}$  completely overlaps with the microburst and is therefore the mean microburst counts. Then,  $n_\sigma$  is proportional to the difference between the mean and the maximum microburst amplitude. However, if we use  $A_{1000}$ , the mean background counts no longer overlap with just the microburst, but rather the microburst and the lower surrounding background. The resulting  $A_{1000}$  is lower than  $A_{500}$ —thus the  $A_{1000}$  burst parameter is more sensitive to the microburst.

To test this possible bias, we ran the detection algorithm with three background values:  $A_{500}$ ,  $A_{1000}$ , and  $A_{2000}$  and compared the resulting median distributions. The



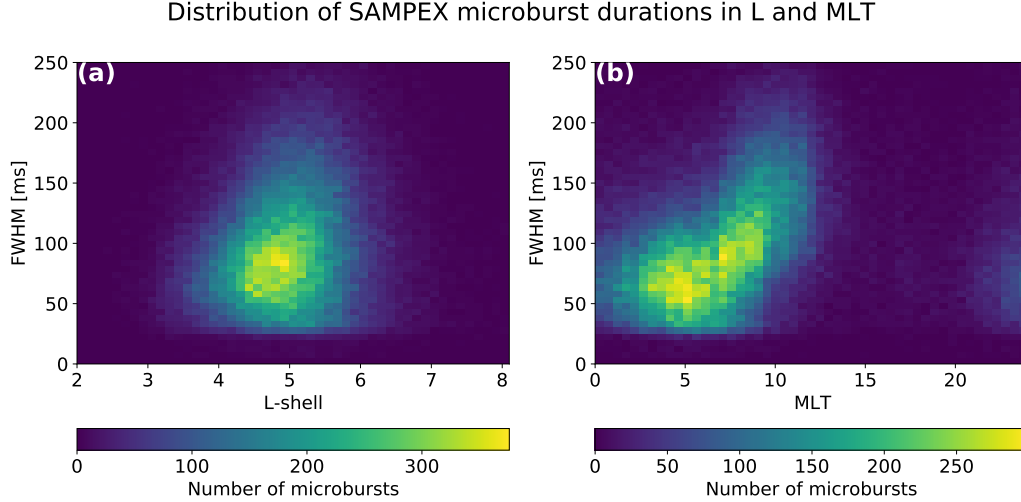


**Figure 4.** The marginalized distributions of the number of microbursts as a function of microburst duration (FWHM) and L shell in panel a, and MLT in panel b.

maximum discrepancy in the median microburst duration, using the three resulting data sets, was 20 ms—one HILT sample. This is a 20% relative discrepancy. Consequently, considering this bias and the distribution in Fig. 2a, the evidence supports that the majority of  $> 1$  MeV microbursts have a true duration around 100 ms and the  $A_{500}$  is adequate to identify them. With more confidence in the detection algorithm, we now discuss the global distribution of microburst durations.

The microburst duration trend in L-shell is subtle; Fig. 3c, and Fig. 4a most clearly show longer durations at higher L-shells near midnight MLT. In contrast, the duration trend in MLT is significant. The median microburst duration doubles from 80 to 160 ms between midnight and noon MLT. Now we will focus on the MLT trend and look for a possible explanation.

As mention in the introduction, chorus rising tone elements are widely believed to scatter microburst electrons (e.g. Breneman et al., 2017; Saito et al., 2012; Miyoshi et al., 2020). Thus, we will compare the microburst duration and chorus trends in local time. Recent studies by Teng et al. (2017) and Shue et al. (2019) quantified the properties of equatorial lower band (0.1-0.5 x electron gyrofrequency) chorus rising tone elements. Both studies found that the rising tone element duration distribution peaks at  $\approx 250$  ms around midnight, and broadening and shifting to  $\approx 500$  ms at noon. The microburst and chorus rising tone element durations double between midnight and noon MLT, but the chorus rising tone element duration is roughly 3 times longer than the relativistic microbursts. However, theory points to a different chorus property controlling the microburst duration.

Figure 4 in Chen et al. (2020) shows the result of a microburst test particle simulation. The authors described what wave properties bound the microburst duration in time-energy space. Medium energy ( $\approx 50$ – $300$  keV) microburst duration is controlled by the rising tone element bandwidth. Moreover, higher energy microburst duration is controlled by the wave’s lower frequency and the upper magnetic latitude of propagation. This is in qualitative agreement with the cyclotron resonance condition described in Lorentzen et al. (2001), and the electron time of flight described by Saito et al. (2012).



While different model configurations may change what wave properties are theoretically responsible for scattering  $> 1$  MeV microburst electrons, it is worth noting that Figs. 4 and 5 in Shue et al. (2019) do not show a clear shift in chorus bandwidth between midnight and noon MLT. Presently, the theory does not conclusively predict what chorus wave properties control the  $> 1$  MeV microburst duration, but the chorus rising tone duration trend in MLT is worth further consideration.

As for the AE trend, the median microburst duration decreases from 130 ms, for  $AE < 100$  nT, to 95 ms for  $AE > 300$  nT. The chorus rising tone duration trend, quantified by Teng et al. (2017), is similar: it is broad and peaks at  $\approx 500$  ms for  $AE < 100$  nT, then narrows and shifts to  $\approx 250$  ms for  $AE > 300$  nT. While both tend to become shorter with increased AE, the scaling factors are different.

Lastly, high latitude chorus waves, found at  $\approx 10^\circ - 25^\circ$  magnetic latitude off of the equator, can also play an important role at scattering microburst electrons (Lorentzen et al., 2001). Li, Thorne, Angelopoulos, Bortnik, et al. (2009) found that the majority of high latitude chorus waves are constrained to 6-12 MLT. Thus, it is tempting to conclude that the microburst duration trend in MLT can be attributed to the low and high latitude chorus waves. However, because low latitude chorus waves are also observed at 0-12 MLT (Li, Thorne, Angelopoulos, Bortnik, et al., 2009), the resulting microburst duration distribution would reflect the chorus wave superposition in the 6-12 MLT region. If low and high latitude chorus waves scattered microbursts with different durations, Fig. 4b would show the microburst durations broaden or bifurcate from midnight to noon MLT. Because Fig. 4b shows the microburst duration only shift to longer durations, high vs low latitude chorus waves are an unlikely explanation for the microburst duration trend in MLT.

In summary, we found that the relativistic microburst duration distribution is peaked at 100 ms, with 75% of microbursts narrower than 140 ms. We found no significant trend in the microburst duration as a function of L-shell, but we did find a strong trend as a function of MLT—the median microburst duration roughly doubles from 80 ms at midnight, to 160 ms at noon MLT. We found that the microburst and chorus rising tone element durations double in MLT, but the rising tone element duration is longer. Nonetheless, at this time theory is inconclusive: it does not predict that the relativistic microburst duration is controlled by the rising tone element duration, but rather by the chorus bandwidth and/or the upper latitude of propagation.

## Acknowledgments

We are thankful for the engineers and scientists who made the SAMPEX mission possible. M. Shumko acknowledges the support provided by the NASA Postdoctoral Program at the NASA's Goddard Space Flight Center, administered by Universities Space Research Association under contract with NASA; L. Blum acknowledges the Heliophysics Innovation Fund program at NASA's Goddard Space Flight Center; and **Alex's funding sources** The SAMPEX HILT and attitude data are located at <http://www.srl.caltech.edu/sampex/DataCenter/data.html> and the minute cadence Auroral Electrojet data is located at [ftp://ftp.ngdc.noaa.gov/STP/GEOMAGNETIC\\_DATA/INDICES/AURORAL\\_ELECTROJET/ONE.MINUTE/](ftp://ftp.ngdc.noaa.gov/STP/GEOMAGNETIC_DATA/INDICES/AURORAL_ELECTROJET/ONE.MINUTE/). This analysis software is available at: [https://github.com/mshumko/sampex\\_microburst\\_widths](https://github.com/mshumko/sampex_microburst_widths), and is archived at **CLEAN UP CODE! Zenodo link (Clean up and document repo before v1.0 release is linked to Zenodo)**.

## References

- Anderson, K. A., & Milton, D. W. (1964). Balloon observations of X rays in the auroral zone: 3. High time resolution studies. *Journal of Geophysical Research*, 69(21), 4457–4479. Retrieved from <http://dx.doi.org/10.1029/>

- JZ069i021p04457 doi: 10.1029/JZ069i021p04457
- Baker, D. N., Mason, G. M., Figueroa, O., Colon, G., Watzin, J. G., & Aleman, R. M. (1993). An overview of the solar anomalous, and magnetospheric particle explorer (SAMPEX) mission. *IEEE Transactions on Geoscience and Remote Sensing*, 31(3), 531–541.
- Blake, J. B., Looper, M. D., Baker, D. N., Nakamura, R., Klecker, B., & Hovestadt, D. (1996). New high temporal and spatial resolution measurements by sampex of the precipitation of relativistic electrons. *Advances in Space Research*, 18(8), 171–186. Retrieved from <http://www.sciencedirect.com/science/article/pii/0273117795009698> doi: [http://dx.doi.org/10.1016/0273-1177\(95\)00969-8](http://dx.doi.org/10.1016/0273-1177(95)00969-8)
- Blum, L., Li, X., & Denton, M. (2015). Rapid MeV electron precipitation as observed by SAMPEX/HILT during high-speed stream-driven storms. *Journal of Geophysical Research: Space Physics*, 120(5), 3783–3794. Retrieved from <http://dx.doi.org/10.1002/2014JA020633> (2014JA020633) doi: 10.1002/2014JA020633
- Breneman, A., Crew, A., Sample, J., Klumpar, D., Johnson, A., Agapitov, O., ... others (2017). Observations directly linking relativistic electron microbursts to whistler mode chorus: Van allen probes and FIREBIRD II. *Geophysical Research Letters*.
- Chen, L., Breneman, A. W., Xia, Z., & Zhang, X.-j. (2020). Modeling of bouncing electron microbursts induced by ducted chorus waves. *Geophysical Research Letters*, 47(17), e2020GL089400. Retrieved from <https://agupubs.onlinelibrary.wiley.com/doi/abs/10.1029/2020GL089400> (e2020GL089400 10.1029/2020GL089400) doi: <https://doi.org/10.1029/2020GL089400>
- Crew, A. B., Spence, H. E., Blake, J. B., Klumpar, D. M., Larsen, B. A., O'Brien, T. P., ... Widholm, M. (2016). First multipoint in situ observations of electron microbursts: Initial results from the NSF FIREBIRD II mission. *Journal of Geophysical Research: Space Physics*, 121(6), 5272–5283. Retrieved from <http://dx.doi.org/10.1002/2016JA022485> (2016JA022485) doi: 10.1002/2016JA022485
- Datta, S., Skoug, R., McCarthy, M., & Parks, G. (1997). Modeling of microburst electron precipitation using pitch angle diffusion theory. *Journal of Geophysical Research: Space Physics*, 102(A8), 17325–17333.
- Douma, E., Rodger, C., Blum, L., O'Brien, T., Clilverd, M., & Blake, J. (2019). Characteristics of relativistic microburst intensity from sampex observations. *Journal of Geophysical Research: Space Physics*.
- Douma, E., Rodger, C. J., Blum, L. W., & Clilverd, M. A. (2017). Occurrence characteristics of relativistic electron microbursts from SAMPEX observations. *Journal of Geophysical Research: Space Physics*, 122(8), 8096–8107. Retrieved from <http://dx.doi.org/10.1002/2017JA024067> (2017JA024067) doi: 10.1002/2017JA024067
- Duderstadt, K. A., Huang, C.-L., Spence, H. E., Smith, S., Blake, J. B., Crew, A. B., ... Vitt, F. M. (2021). Estimating the impacts of radiation belt electrons on atmospheric chemistry using firebird ii and van allen probes observations. *Journal of Geophysical Research: Atmospheres*, n/a(n/a), e2020JD033098. Retrieved from <https://agupubs.onlinelibrary.wiley.com/doi/abs/10.1029/2020JD033098> (e2020JD033098 2020JD033098) doi: <https://doi.org/10.1029/2020JD033098>
- Horne, R. B., & Thorne, R. M. (2003). Relativistic electron acceleration and precipitation during resonant interactions with whistler-mode chorus. *Geophysical Research Letters*, 30(10). Retrieved from <http://dx.doi.org/10.1029/2003GL016973> (1527) doi: 10.1029/2003GL016973
- Johnson, A., Shumko, M., Griffith, B., Klumpar, D., Sample, J., Springer, L., ...

- others (2020). The FIREBIRD-II CubeSat mission: Focused investigations of relativistic electron burst intensity, range, and dynamics. *Review of Scientific Instruments*, 91(3), 034503.
- Klecker, B., Hovestadt, D., Scholer, M., Arbing, H., Ertl, M., Kastele, H., . . . others (1993). HILT: A heavy ion large area proportional counter telescope for solar and anomalous cosmic rays. *IEEE transactions on geoscience and remote sensing*, 31(3), 542–548.
- Kurita, S., Miyoshi, Y., Blake, J. B., Reeves, G. D., & Kletzing, C. A. (2016). Relativistic electron microbursts and variations in trapped mev electron fluxes during the 8–9 october 2012 storm: Sampex and van allen probes observations. *Geophysical Research Letters*, 43(7), 3017-3025. Retrieved from <https://agupubs.onlinelibrary.wiley.com/doi/abs/10.1002/2016GL068260> doi: <https://doi.org/10.1002/2016GL068260>
- Li, W., Thorne, R., Angelopoulos, V., Bonnell, J., McFadden, J., Carlson, C., . . . Auster, H. (2009). Evaluation of whistler-mode chorus intensification on the nightside during an injection event observed on the THEMIS spacecraft. *Journal of Geophysical Research: Space Physics*, 114(A1).
- Li, W., Thorne, R. M., Angelopoulos, V., Bortnik, J., Cully, C. M., Ni, B., . . . Magnes, W. (2009). Global distribution of whistler-mode chorus waves observed on the THEMIS spacecraft. *Geophysical Research Letters*, 36(9). Retrieved from <http://dx.doi.org/10.1029/2009GL037595> (L09104) doi: 10.1029/2009GL037595
- Lorentzen, K. R., Blake, J. B., Inan, U. S., & Bortnik, J. (2001). Observations of relativistic electron microbursts in association with VLF chorus. *Journal of Geophysical Research: Space Physics*, 106(A4), 6017–6027. Retrieved from <http://dx.doi.org/10.1029/2000JA003018> doi: 10.1029/2000JA003018
- Meredith, N. P., Horne, R. B., Shen, X.-C., Li, W., & Bortnik, J. (2020). Global model of whistler mode chorus in the near-equatorial region ( $|\lambda_m| < 18^\circ$ ). *Geophysical Research Letters*, 47(11), e2020GL087311.
- Miyoshi, Y., Saito, S., Kurita, S., Asamura, K., Hosokawa, K., Sakanoi, T., . . . others (2020). Relativistic electron microbursts as high energy tail of pulsating aurora electrons.
- O’Brien, T. P., Looper, M. D., & Blake, J. B. (2004). Quantification of relativistic electron microburst losses during the GEM storms. *Geophysical Research Letters*, 31(4). Retrieved from <http://dx.doi.org/10.1029/2003GL018621> (L04802) doi: 10.1029/2003GL018621
- O’Brien, T. P., Lorentzen, K. R., Mann, I. R., Meredith, N. P., Blake, J. B., Fennell, J. F., . . . Anderson, R. R. (2003). Energization of relativistic electrons in the presence of ULF power and MeV microbursts: Evidence for dual ULF and VLF acceleration. *Journal of Geophysical Research: Space Physics*, 108(A8). Retrieved from <http://dx.doi.org/10.1029/2002JA009784> doi: 10.1029/2002JA009784
- Ripoll, J.-F., Claudepierre, S., Ukhorskiy, A., Colpitts, C., Li, X., Fennell, J., & Crabtree, C. (2020). Particle dynamics in the earth’s radiation belts: Review of current research and open questions. *Journal of Geophysical Research: Space Physics*, 125(5), e2019JA026735.
- Saito, S., Miyoshi, Y., & Seki, K. (2012). Relativistic electron microbursts associated with whistler chorus rising tone elements: Gensis-rbw simulations. *Journal of Geophysical Research: Space Physics*, 117(A10), n/a–n/a. Retrieved from <http://dx.doi.org/10.1029/2012JA018020> (A10206) doi: 10.1029/2012JA018020
- Seppälä, A., Douma, E., Rodger, C., Verronen, P., Clilverd, M. A., & Bortnik, J. (2018). Relativistic electron microburst events: Modeling the atmospheric impact. *Geophysical Research Letters*, 45(2), 1141–1147.
- Shue, J.-H., Nariyuki, Y., Katoh, Y., Saito, S., Kasahara, Y., Hsieh, Y.-K., . . . Goto,

- 410 Y. (2019). A systematic study in characteristics of lower band rising-tone  
411 chorus elements. *Journal of Geophysical Research: Space Physics*, 124(11),  
412 9003–9016.
- 413 Shumko, M., Johnson, A. T., O’Brien, T. P., Turner, D. L., Greeley, A. D., Sam-  
414 ple, J. G., ... Halford, A. J. (2020). Statistical properties of electron cur-  
415 tain precipitation estimated with aerocube-6. *Journal of Geophysical Re-*  
416 *search: Space Physics*, 125(12), e2020JA028462. Retrieved from [https://](https://agupubs.onlinelibrary.wiley.com/doi/abs/10.1029/2020JA028462)  
417 [agupubs.onlinelibrary.wiley.com/doi/abs/10.1029/2020JA028462](https://agupubs.onlinelibrary.wiley.com/doi/abs/10.1029/2020JA028462)  
418 (e2020JA028462 10.1029/2020JA028462) doi: [https://doi.org/10.1029/](https://doi.org/10.1029/2020JA028462)  
419 2020JA028462
- 420 Shumko, M., Turner, D. L., O’Brien, T. P., Claudepierre, S. G., Sample, J.,  
421 Hartley, D. P., ... Mitchell, D. G. (2018). Evidence of microbursts ob-  
422 served near the equatorial plane in the outer van allen radiation belt. *Geo-*  
423 *physical Research Letters*, 45(16), 8044-8053. Retrieved from [https://](https://agupubs.onlinelibrary.wiley.com/doi/abs/10.1029/2018GL078451)  
424 [agupubs.onlinelibrary.wiley.com/doi/abs/10.1029/2018GL078451](https://agupubs.onlinelibrary.wiley.com/doi/abs/10.1029/2018GL078451) doi:  
425 10.1029/2018GL078451
- 426 Summers, D. (2005). Quasi-linear diffusion coefficients for field-aligned electro-  
427 magnetic waves with applications to the magnetosphere. *Journal of Geophys-*  
428 *ical Research: Space Physics*, 110(A8), n/a–n/a. Retrieved from [http://](http://dx.doi.org/10.1029/2005JA011159)  
429 [dx.doi.org/10.1029/2005JA011159](http://dx.doi.org/10.1029/2005JA011159) (A08213) doi: 10.1029/2005JA011159
- 430 Teng, S., Tao, X., Xie, Y., Zonca, F., Chen, L., Fang, W., & Wang, S. (2017). Anal-  
431 ysis of the duration of rising tone chorus elements. *Geophysical Research Let-*  
432 *ters*, 44(24), 12–074.
- 433 Thébault, E., Finlay, C. C., Beggan, C. D., Alken, P., Aubert, J., Barrois, O., ...  
434 others (2015). International geomagnetic reference field: the 12th generation.  
435 *Earth, Planets and Space*, 67(1), 79.
- 436 Thorne, R. M. (2010). Radiation belt dynamics: The importance of wave-particle in-  
437 teractions. *Geophysical Research Letters*, 37(22). Retrieved from [http://](http://dx.doi.org/10.1029/2010GL044990)  
438 [dx.doi.org/10.1029/2010GL044990](http://dx.doi.org/10.1029/2010GL044990) (L22107) doi: 10.1029/2010GL044990
- 439 Thorne, R. M., O’Brien, T. P., Shprits, Y. Y., Summers, D., & Horne, R. B. (2005).  
440 Timescale for MeV electron microburst loss during geomagnetic storms. *Jour-*  
441 *nal of Geophysical Research: Space Physics*, 110(A9). Retrieved from [http://](http://dx.doi.org/10.1029/2004JA010882)  
442 [dx.doi.org/10.1029/2004JA010882](http://dx.doi.org/10.1029/2004JA010882) (A09202) doi: 10.1029/2004JA010882
- 443 Winckler, J., Bhavsar, P., & Anderson, K. (1962). A study of the precipitation of  
444 energetic electrons from the geomagnetic field during magnetic storms. *Journal*  
445 *of Geophysical Research*, 67(10), 3717–3736.